4-dimensional Local Radial Basis Function Interpolation of Large, Uniformly Spaced Datasets

J.Thewlis, D.Stevens, H.Power, D.Giddings, P.Gowland, M.Vloeberghs

Abstract

Background and Objective

Large, uniformly spaced, complex and time varying datasets derived from high resolution medical image velocimetry can provide a wealth of information regarding small scale transient physiological flow phenomena and pulsation of anatomical boundaries. However, there remains a need for interpolation techniques to effectively reconstruct a fully 4-dimensional functional relationship from this data. This paper presents a preliminary evaluation of a 4-dimensional local radial basis function (RBF) algorithm as a means of addressing this problem for laminar flows.

Methods

A 4D interpolation algorithm is proposed based on a Local Hermitian Interpolation (LHI) using a combination of multi-quadric RBF with a partition of unity scheme. The domain is divided into uniform sub-systems with size restricted to immediately neighbouring points. The validity of the algorithm is first established on a known 4D analytical dataset. Application is then demonstrated through characterisation of a large 4D flow velocity dataset obtained from magnetic resonance imaging (MRI) measurements of cerebrospinal fluid flow in the brain.

Results

Performance of the algorithm is compared to that of a quad-linear interpolation, demonstrating favourable improvement in accuracy. The technique is shown to be robust, computationally efficient and capable of refined interpolation in Euclidean space and time. Application to MR velocimetry data is shown to produce promising results for the 4D reconstruction of the transient flow field and movement of the fluid boundaries at spatial and temporal locations intermediate to the original data.

Conclusion

This study has demonstrated feasibility of an accurate, stable and efficient 4-dimensional local RBF interpolation method for large, transient laminar flow velocimetry datasets. The proposed approach does not suffer from ill-conditioning or high computational cost due to domain decomposition into local stencils where the RBF is only ever applied to a limited number of points. This work offers a potential tool to assist medical diagnoses and drug delivery through better understanding of physiological flow fields such as cerebrospinal fluid. Further work will evaluate the technique on a wider range of flow fields and against CFD simulation.

Keywords: radial basis function, image reconstruction, cerebrospinal fluid,

1 Introduction

High-resolution magnetic resonance imaging (MRI) techniques can be used to acquire measurements of small-scale flow velocity data in the human body over a large number of spatio-temporal points at regularly spaced intervals. There is a need to develop a method of generating an interpolation field

that allows a prediction of information lying between MRI voxels, and at times intermediate to the MRI image samples, which are described for example, in [1], [2], [3], [4], [5] in which the challenge of analysing the fluid motion in cerebrospinal fluid is considered. These flow fields are typically slow moving, highly non-linear, pulsatile and can vary strongly on length-scales of just a few voxels. However, understanding this behaviour is critical to the treatment of severe pathologies such as hydrocephalus. This therefore motivates the employment of a high-order image interpolation approach.

Reviews by [6] and [7] evaluated the majority of 2 and 3-dimensional scattered data interpolation methods available in terms of storage, accuracy, visual pleasantness and ease of implementation, concluding that methods based on radial basis function (RBF) collocation, in particular the multiquadric RBF developed by [8], represent the most effective approach in most cases. These methods are particularly attractive for interpolation of higher-dimensional datasets and are also well suited to handling irregular datasets. An RBF can be defined as a real-valued function depending only on distance from a fixed location. The use of RBF collocation methods is commonplace in several industrial and academic disciplines including surface reconstruction [8], image processing [9], [10], [11] and neural networks [12], [13].

Since radial basis functions depend only on separation distance between data centres and reconstruction locations, the procedure remains identical in any number of dimensions; only computation of the separation distance changes. By contrast, high-order polynomial interpolation becomes increasingly complex the higher the dimension. Interpolation schemes for datasets in more than 2 dimensions therefore typically rely on linear interpolation of each spatial dimension. Full-domain RBF methods exhibit flexibility and high order convergence rates. However, there are problems with poor numerical conditioning and high computational cost [7], [14]. [15] described this as the uncertainty relation: better conditioning is associated with worse accuracy, and worse conditioning is associated with improved accuracy. This problem becomes more apparent the greater the size of the system and has restricted applications to smaller and/or lower dimensional order datasets.

Scalable alternatives to the multiquadric RBF have been developed; for example, the compact support approach [16], [17]. However, the support size and the functions employed vary depending on the number of dimensions since the method is based on a polynomial approximation to truncated RBFs. Therefore, the computational cost and complexity of the method are significantly increased when applied in higher dimensions. In contrast, the multiquadric RBF can be scaled naturally to higher dimensions without alteration, although the uncertainty relation remains a problem. In order to address this, several methods have been developed. For example, RBF-specific preconditioners [18] and adaptive selection of data centres [19]. However, the only reliable method currently available is domain decomposition [19], [20], [21], [22], [23].

Localised RBF collocation methods such as those of [24] and [25] have since been developed. These methods allow significantly more efficient interpolation of large scattered datasets by employing domain decomposition to divide the domain into a series of small and overlapping sub-systems centred around each collocation point. For each point, the interpolation function is evaluated only on the associated sub-domain, instead of the global domain. A global function characterising the overall domain is then generated as the weighted sum of the locally interpolated functions. As each individual RBF sub-system never grows too large, these methods can be scaled to arbitrarily large datasets

without numerical conditioning issues, and without losing the natural scalability to higher dimensions inherent in full-domain RBF collocation. At the expense of creating some localised connectivity, the flexibility of working with a scattered dataset can be retained.

Localised methods have also been used in the solution of partial differential equations [26]. In [27] [28], [29], [30], a Local Hermitian Interpolation (LHI) method is described which is capable of operating on a variety of 2 and 3D scattered data-sets with arbitrary boundary conditions. More recently, [31] applied a local RBF method to 2-dimensional inverse Cauchy problems, and [32] to the solution of 2-dimensional incompressible Navier-Stokes equations.

The fundamentals of these local RBF collocation methods may be adapted for the interpolation of higher-dimension data fields. Recent work [33], [34] demonstrates that by using a k-d tree based search algorithm to assign scattered points to local systems based on a combination of the compactly supported Wendland RBFs with a partition of unity weighting scheme (PUM), an effective interpolation can be achieved for $D > 3$. Stable and accurate results are presented up to 5D. Capability to deal with scattered data of varying density has since been developed using an algorithm to adaptively vary the sizes of each local system [35].

In this work we consider the development of an alternative 4-dimensional local multiquadric RBF interpolation algorithm for large datasets, first described in [36]. Motivated by the interpolation of MRI velocimetric data, which is highly regular, we describe an approach optimised for computational efficiency on regularly spaced datasets; however, the method itself is equally applicable to the interpolation of irregular data. We use an algorithm based on division of the domain into uniform local stencils, in combination with a local partition of unity scheme. Search size is restricted to immediately neighbouring points to control ill conditioning. We can then take advantage of the scalability of the multiquadric RBF to higher dimensions.

There is only limited precedent for application of higher order RBF interpolation to flow velocity and or geometric based medical image data. [37] uses a 3D Gaussian global RBF interpolation on a relatively small unstructured particle image velocimetry dataset. [9] used an RBF technique to interpolate a localised velocity field resulting from sparse MRI data in the arch of the aorta. [10] uses a method of variational implicit surfaces using thin plate spline RBFs to perform 3D interpolation of cardiac geometry from coarse MR images. [11] uses a combination of level set method with RBF for segmentation and interpolation of structural contours from 3D MRI contrast images over a cardiac cycle. This method can produce refined images of anatomical boundaries in 4D. However, each of the above cases is limited by the use of global RBFs. The techniques have largely been demonstrated on relatively small, lower order datasets and the size of datasets that can be handled may be limited by ill conditioning and computational cost.

[38] and [39] have used alternative 2 and 3D spatial RBF based methods for interpolation of sparse haemodynamic MRI data, imposing a divergence free fluid mechanics limitation to remove wall effects and imaging noise prior to interpolation. However, this approach has again been based on globally applied, lower order RBFs. The divergence free criterion has not been considered for our application, since due to the influence of porous sub-pixel structures, i.e. subarachnoid granulations or choroid plexus, CSF flow cannot be considered strictly divergence free at the wall boundary. Divergence free constraints may also be affected by small-scale variation in position of the ventricle boundaries. We have instead accounted for noise at the fluid boundaries through a standard least squares rigid body motion removal algorithm.

Recent approaches have focussed around use of machine learning techniques to predict missing information from sparse or incomplete medical image data, with the aim of reducing scan times. Some examples exist of the use of global RBF interpolation within these methods, such as [12] where a FCM (fuzzy C-means) neural network approach is used in conjunction with RBF interpolation to segment brain structures on 2D planes. In [13], RBFs are used as a component within an enhanced fuzzy neural network to enable improved MRI image interpolation from 2D slices and interpret ambiguities caused by noise. However, the application of the RBF in these methods is on the hidden nodes of the neural network and not the velocity field in the images. Methods not involving RBF interpolation include [40], where a bidirectional recurrent convolutional neural network with a refine network of 2D convolutions in-plane has been used to reconstruct image data of the knee and brain with high accuracy.

In general, a large amount of historic image data is required to train neural networks and the authors acknowledge a significant computational cost to this training phase and subsequent running of their algorithm. More recently, [41] has demonstrated an alternative deep neural network based solution involving using 4D MR velocimetry data as a direct input to the solution of the 4D PDEs of the Navier Stokes equations using automatic differentiation, enabling direct characterisation of the pressure field without a separate numerical model and significantly reduced computational cost.

These methods provide powerful tools to enable comprehensive interpretation of internal structures and flow fields from incomplete image datasets but rely on the availability of a significant quantity of good quality historic data for their training. We believe our 4D method offers an alternative, highly accurate reconstruction from small scale refined data that can easily be scaled to higher dimensions at low computational cost, without loss of stability and without the need for training or prior knowledge of the dataset.

2 4D Local RBF collocation method for uniformly spaced data

Data connectivity based on a regular rectilinear 4D Cartesian grid *x, y, z, t* structure, such as the pixel-based form taken by medical image data, lends itself well to a stencil based local RBF formulation. Stencils are formed by connecting each node at which functional values are known to its immediate neighbours within the Cartesian grid structure. Each stencil therefore consists of 81 nodes for a four-dimensional dataset, and the entire solution domain is covered by overlapping stencils. Stencils are not formed at boundary nodes, in order to maintain a consistent stencil size and shape throughout the domain. The method does not require that the dataset be uniform, only that the dataset be regular. However, if the nodal separation in any one direction differs substantially, scaling is applied in order to keep the aspect ratio of the local stencils close to 1. For data with a spatial and temporal aspect, this will typically require scaling of the time variable such that the time step size is of the same order as the spatial separations. To determine points associated with each stencil, a search algorithm is used whereby the domain is divided into evenly spaced boxes equal to the total number of stencils. Points are allocated boxes based on their fraction of the overall range of data in each dimension. The number of points in each box is counted and these values along with the array indices of each point are stored for later use in constructing the local RBF collocations.

The RBF interpolation is evaluated only on the points in a local stencil rather than across the entire domain. Since the domain is covered by overlapping RBF systems, each reconstruction location can be expected to lie within the domain of several neighbouring collocation systems. In order to produce a

smoothly varying and consistent global reconstruction of the data field it is therefore necessary to assign a relative weight to the estimate from each contributing system, i.e. a standard "partition of unity" reconstruction [33]. The effect of choosing different weighting schemes is considered in section 2.1.

We consider the multiquadric radial basis function,

$$\psi(r) = (r^2 + c^2)^{1/2}$$

Equation 1

Here r is a length scale representing radial separation distance between points found in a given local stencil. Since 4 dimensions are considered, $r^2=r_x^2+r_y^2+r_z^2+r_t^2$. The c term is the RBF shape parameter, which controls the relative flatness of the basis function. This parameter is a length scale which may be tuned to optimise the interpolation function based on the size of the domain and the shape of the interpolating function. Variation of this parameter is considered in section 2.1.

For each local system, the multiquadric RBF collocation procedure builds an interpolation function $\emptyset(x)$ for a given data centre, x as a weighted sum of radial basis functions evaluated at a set of N chosen neighbouring functional centres, ξ_j, that are distributed over the local interpolation domain, plus a polynomial term of order 0 (*Equation 2*), with NP the number of terms in the polynomial, (here *NP=1*):

$$\emptyset(x) = \sum_{j=1}^{N} \alpha_j \psi(\|x - \xi_j\|) + \sum_{j=1}^{NP} \alpha_{j+N} P_j^0(x)$$

Equation 2

By enforcing the interpolation function, *Equation 1*, at all locations where the solution is known, x_i, we obtain a linear system of equations which may be solved to obtain the functional coefficients α_j:

$$\phi(x_i) = \sum_{j=1}^{N} \alpha_j \psi(\|x_i - \xi_j\|) + \sum_{j=1}^{NP} \alpha_{j+N} P_j^0(x_i)$$

Equation 3

Along with the constant polynomial constraint condition (*Equation 4*), i.e.:

$$\sum_{j=1}^{N} \alpha_j P_k^0(x_j) = 0 \qquad k = 1, \dots, \mathrm{NP}$$

Equation 4

The full formulation of this problem can be expressed in the form $[A][\alpha] = [b]$, where:

$$[A] = \begin{pmatrix} \psi & P^0 \\ P^{0T} & 0 \end{pmatrix}$$

$$[b]^T = ([\phi(x_i)], \quad [0])$$

Equation 5

Here $\emptyset(x_i)$ are the known values of the field variable $\emptyset$ at the data centres x_i. We identify this as the data vector for the local collocation system. ψ_{ij} is identified as the collocation matrix for the local RBF system and defines the relationship, in terms of the chosen RBF (*Equation 1*), between each data centre x_i, and each of the chosen neighbouring functional centres in the local system, ξ_j. If the number of data centres x_i is of the same size as the number of functional centres, ξ_j, (*N*), then *Equation 5* represents a square system that can be solved directly. Furthermore, if $\{x_i\} = \{\xi_i\}$, i.e. the functional centres are placed only at locations where the field variable is known, then the collocation matrix is symmetric. This is the case for all interpolation systems used in this work since the input image data is uniformly populated and is the most used formulation within the literature. The ability to define the functional centres in locations within the local domain other than the known data centres can be of benefit in evaluating scattered input data, where points maybe unevenly distributed. However, this is not considered here.

Having obtained the functional coefficients α_j via the solution of *Equation* , the value of the interpolation function at any reconstruction location $\bar{x}$ within the local interpolation domain may be obtained by applying the RBF reconstruction formula *Equation 2*. Writing this as a vector product we have:

$$\phi(\bar{x}) = R_j(\bar{x})\alpha_j$$

Equation 6

where the vector $R_j(\bar{x})$ is defined by:

$$R_j(\bar{x}) = \psi\left(\left\|\bar{x} - \xi_j\right\|\right)$$

Equation 7

The procedure to obtain the functional coefficients α_j requires the solution of a linear system of equations with local data values on the right hand side; see *Equation* . However, for our application it is more computationally efficient to use instead a reconstruction weights vector that can multiply directly with the data vector ϕ_i. To do this we solve the matrix system

$$\psi_{ij}W_i(\bar{x}) = R_j(\bar{x})$$

Equation 8

in order to obtain the vector $W_i(\bar{x})$, which we identify as the reconstruction weights vector for position $\bar{x}$. With this vector $W_i(\bar{x})$ we may obtain the value of the interpolation function at $\bar{x}$ via simple multiplication with the data vector:

$$\phi(\bar{x}) = W_i(\bar{x})\phi_i$$

Equation 9

An RBF collocation system is defined for each local stencil. However, since the RBF method relies only on relative nodal separations, we may exploit the regular Cartesian grid structure to enhance computational efficiency by forming only a single RBF collocation system over a template stencil centred at the origin. Operating in this way the individual RBF collocation matrices ψ become identical, and formation of the RBF collocation systems becomes a pre-processing operation. Similarly, reconstruction weights W determined by the RBF collocation may be stored for every potential interpolation location within the template system and reused many times. A multiplication

of the stencil weights with a local data-vector is all that is then required in order to reconstruct the field-values at each interpolation location, as defined by *Equation* . Solution of the RBF matrix system is only necessary in order to obtain the template reconstruction weights vectors via *Equation* , again as a pre-processing operation.

2.1 Numerical Validation

In this section we compare the proposed 4D RBF collocation to a polynomial interpolation approach using a quad-linear interpolation, i.e. an extension of the well-known bilinear/trilinear interpolation method to four dimensions. We consider the 4-dimensional test function *Equation 3*, over the domain $(x, y, z, t) \in [-1, 1]$, which represents a well behaved continuous transient function with similar characteristics to that of creeping/slow laminar flow. We form a regular Cartesian grid using *N+1* nodes in each direction, such that the separation between adjacent nodes is $2/n$, i.e. forming N^4 voxels within the domain. The data-field is then interpolated to produce an additional four subdivisions in each direction, i.e. to generate an additional 256 sub-voxels within each of the original voxels.

$$\emptyset_e(r) = e^{-r^2} + 0.1cos(4\pi r)$$
$$r = (x^2 + y^2 + z^2 + t^2)^{1/2}$$

Equation 3

Figure 1 demonstrates the effect of varying the RBF shape parameter (see *Equation 1*), using the *N = 20* dataset. As the shape parameter *c* is a length scale it is more convenient to consider the non-dimensional equivalent *c** =*c*/Δ, where Δ is the local nodal separation. The behaviour shown here is typical of RBF collocation methods; the solution accuracy improves as the shape parameter is increased (i.e. as the basis functions are made increasingly flat) until a maximum accuracy is achieved; in this case at around *c** = 0.3. As the shape parameter is increased further the solution accuracy is reduced. While the precise optimal value of *c** will vary depending on the characteristics of the dataset, *c** values in the range 0.1 to 1.0 typically provide close to optimal accuracy for the purposes of 4D interpolation, across a wide variety of interpolation fields.

The shape parameter does not have to take a constant value. Kansa [42] found that a variable shape parameter with a given expansion produced the best results for a multiquadric interpolation. Furthermore, each function in an interpolation formula may be assigned a different value [43]. More recently, strategies for the selection and formulation of variable shape parameters have been investigated [44], [45]. However, although they may be applied to such problems, for a computational domain with a uniform discretisation with little variation, it is appropriate to use a constant shape parameter for each local system [46]. Hence here a sensible value has been selected empirically based on the domain geometry.

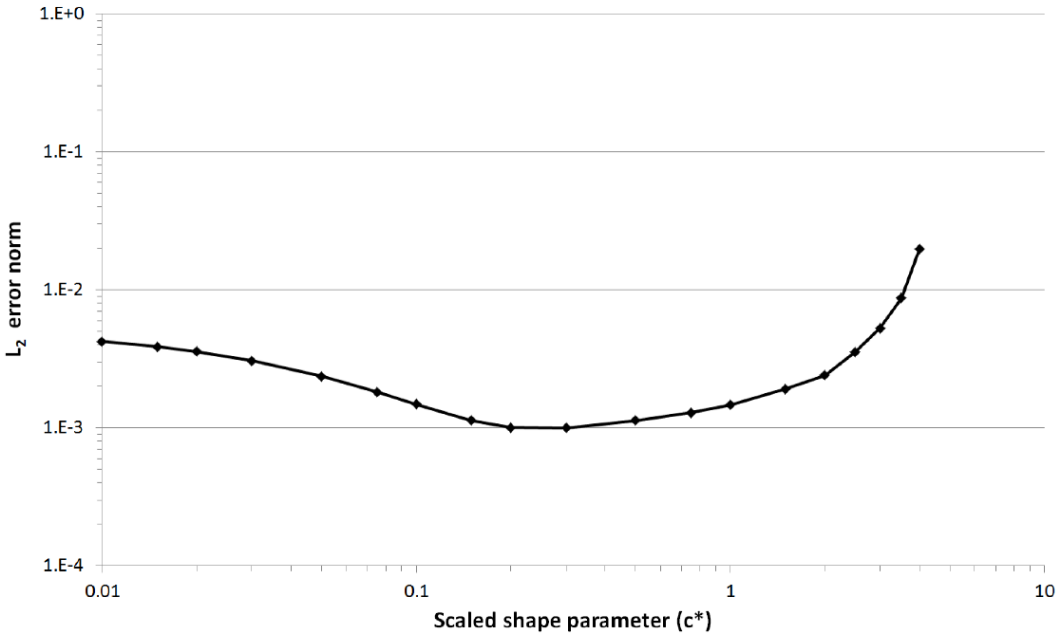

Figure 1 Variation of error with shape parameter: N=20 dataset.

Figure 2 shows the spatial convergence of the proposed RBF approach in comparison to the quad-linear polynomial interpolation, for datasets varying in density between N = 10 and N = 50. The RBF approach offers a clear improvement in accuracy over the polynomial interpolation, which increases as the dataset density is refined; on the finest dataset tested the RBF offers around thirty times the accuracy of the polynomial approach. Examining the rate of spatial convergence numerically, we see a convergence rate of 1.87 for the polynomial, in comparison to a convergence rate of 3.47 for the RBF approach.

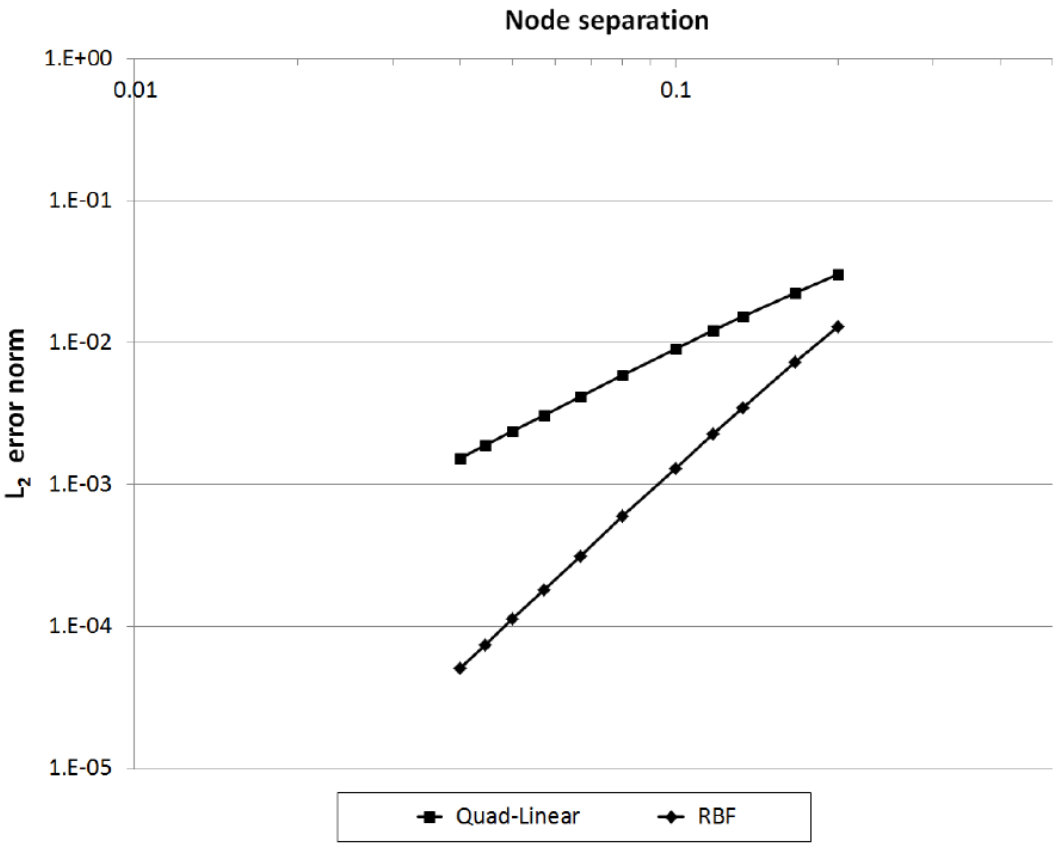

Figure 2 Spatial convergence of RBF and quad-linear interpolation schemes (c = 0.5)*

Figure 3 a) plots the quad linear interpolated value of ∅ against the exact solution, along a diagonal extending from the centre of the domain to the outermost corner of the domain at $x = y = z = t = 1$, for the $N = 10$ dataset. Locations along this line where the solution is known are marked with circles. The RBF interpolation Figure 3 b) shows that the exact solution is represented more accurately when using an RBF interpolation; in particular at peaks and troughs of the function that are far from any "fixing" node. Figure 3 c) and d) show the corresponding results for the $N = 20$ dataset. Here the RBF interpolation function is virtually indistinguishable from the exact solution, whereas the quad-linear interpolation offers a reconstruction quality like that of the RBF case on the coarser dataset.

As discussed in Section 3, when reconstructing at a location that exists within the interpolation domain of several overlapping interpolation systems, it is necessary to construct the final interpolation value as a weighted average of the estimates from the various overlapping systems; i.e. build a partition of unity function [33]. We consider here four weighting approaches for the partition of unity function. The 'uniform weighting' scheme assigns an equal weight to each contributing system. The 'linear decay' and 'quadratic decay' functions consider weights that decay (linearly or quadratically) towards zero at the farthest extent of the stencil. The 'closest node only' scheme assigns a non-zero weight only to the interpolation system that is formed around the closest interior node (if multiple nodes are equidistant from the reconstruction location then both are considered with equal weight). Note that all preceding results in this section have used a uniform weighting approach. Table 1 shows the L_2 errors obtained for these different weighting schemes, using two different datasets ($N = 10$ and $N = 20$), at two different shape parameters ($c^* = 0.1$ and $c^* = 1$). The choice of weighting scheme has only minimal impact on the solution accuracy; in each case the accuracy of the predicted solution is within a few percent between the various reconstruction schemes. The 'closest node only' scheme is of interest, since the vastly reduced number of reconstructions leads to a correspondingly reduced

computational cost. It is important to note, however, that using this scheme will lead to very small 'jumps' in the interpolation function as it moves from the domain of one interpolation stencil to another. Whether or not such jumps in the reconstructed solution field are acceptable will be a problem dependent issue.

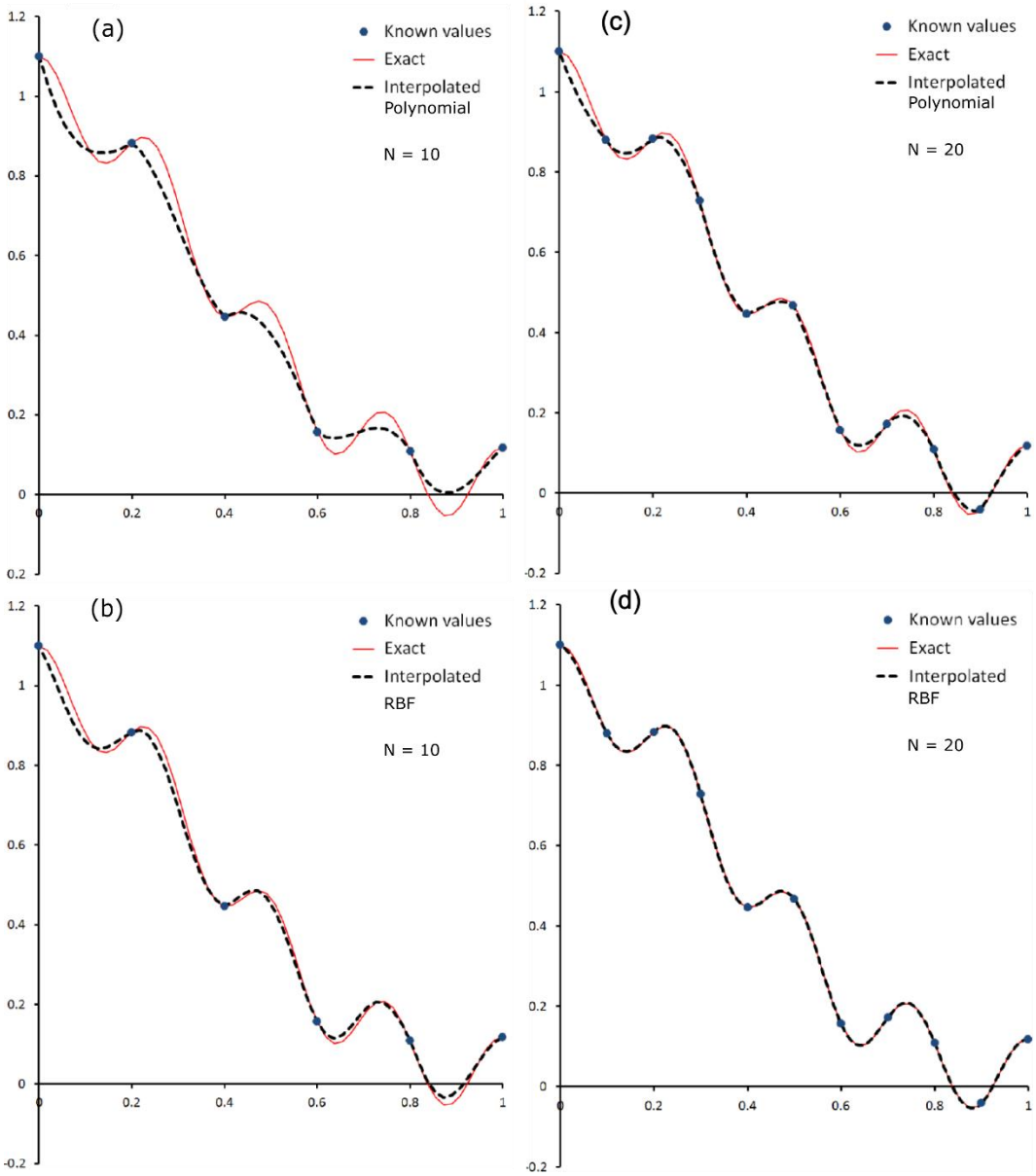

Figure 3 Interpolation function along positive diagonal: N = 10 dataset a) Quad-linear interpolation, N = 10, b) RBF interpolation, N = 10, c) Quad-linear interpolation, N = 20, d) RBF interpolation, N = 20.

Table 1 Comparison of various partition of unity weighting schemes (L_2 error norms shown)

Test case	Uniform weighting	Linear decay	Quadratic decay	Closest node only
$N = 10$, $c^* = 0.1$	1.553×10^{-2}	1.540×10^{-2}	1.530×10^{-2}	1.512×10^{-2}
$N = 10$, $c^* = 1$	1.489×10^{-2}	1.478×10^{-2}	1.470×10^{-2}	1.473×10^{-2}
$N = 20$, $c^* = 0.1$	1.484×10^{-3}	1.382×10^{-3}	1.324×10^{-3}	1.546×10^{-3}

N = 20, c^* = 1	1.464×10^{-3}	1.442×10^{-3}	1.434×10^{-3}	1.576×10^{-3}

2.2 4D CFD Flow Phantom Model

Prior to evaluating the algorithm on real world physiological CSF flow data , we first validate its effectiveness on a 4D CFD flow phantom representing transient laminar flow in a square duct, using the Ansys Fluent CFD solver. Water was chosen as the fluid medium due to its similarity in properties to CSF. A duct of height 10mm and length 200mm was selected to enable full development of the flow. To simulate MR data, a uniformly spaced hexahedral mesh was used without boundary layer growth functions. An initial steady state mesh sensitivity study was conducted, with inlet velocity of $0.1ms^{-1}$ and zero-gauge outlet pressure, resulting in an optimal element size of 0.5mm.

A sinusoidally varying transient inlet function was formulated to ensure initial values of zero velocity, solely positive values over the cycle and an entirely laminar flow regime.

$$u(t) = 0.05\left(sin\left(\frac{3\pi}{2} + 2t\right) + 1\right)$$

The duct flow was then solved transiently over a period of 10s with a time step of 0.01s, covering 3 cycles to allow full development of the flow, again using a zero-gauge outlet pressure condition. Velocity data from this case was collected from cell centres at 20 uniformly spaced planes parallel to the outlet at 20 time intervals of 0.5s to form a 4-dimensional input dataset to test the RBF interpolation. Time data was scaled by 10^{-3} to ensure uniform local systems. This dataset was then interpolated to the inlet boundary of a second laminar duct flow model, identical except for an inclined inlet plane. This case was again solved transiently over a period of 10s and the development of the flow compared to that in the initial model, as shown in Figure 4. Flow at several cross-sectional planes along the duct over the 3rd flow cycle is shown for the initial model and the inclined duct interpolated case. The flow development in the inclined inlet duct shows good agreement with the initial case. Variation of average flow at the duct outlet is plotted in Figure 5 for both cases. Although input data were relatively sparsely located in time, the transient outflow profile is still reconstructed accurately.

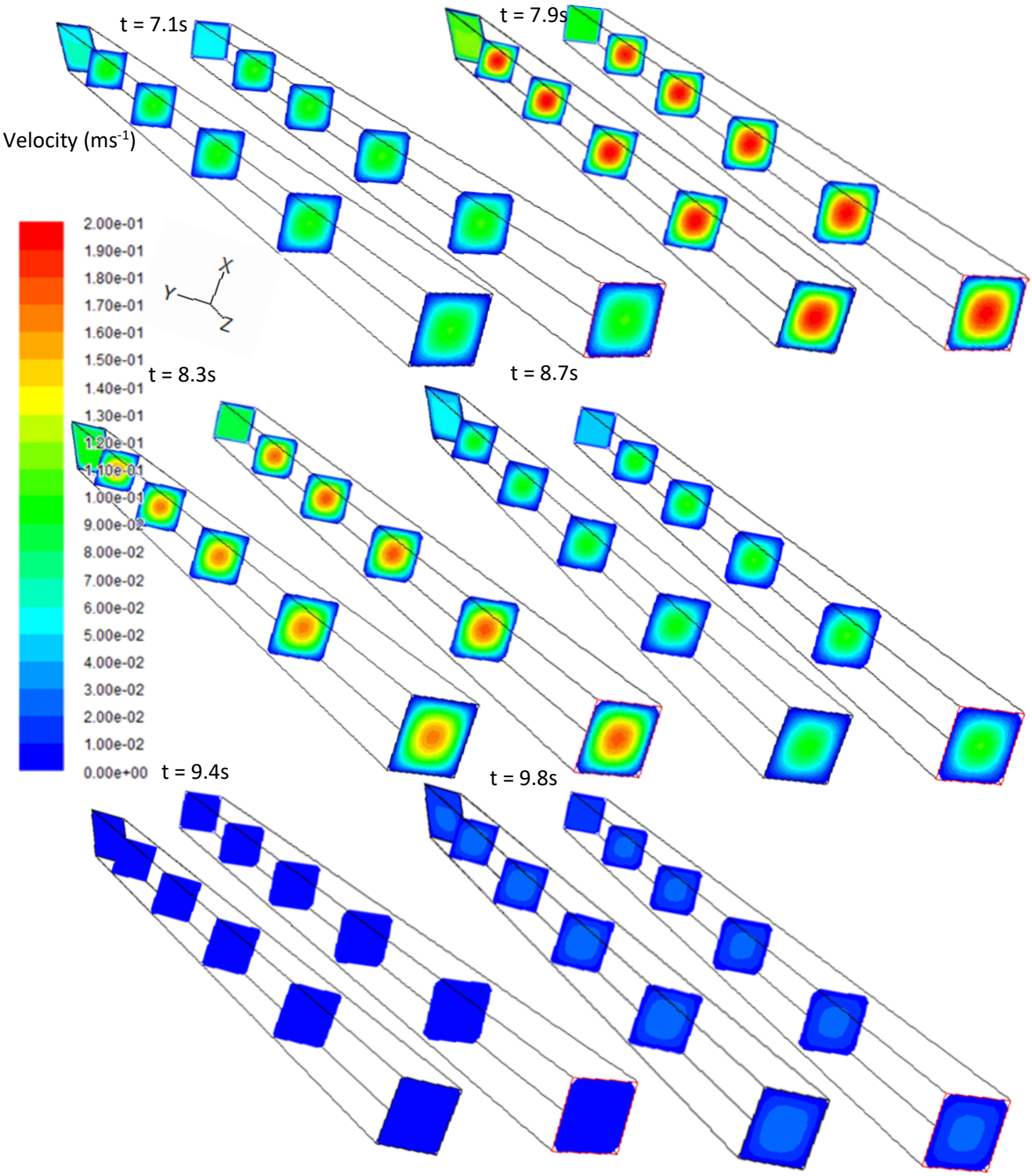

Figure 4 Contours of velocity at several cross sections of full duct, and truncated inclined entrance duct simulation over cycle at times 7.1 s, 7.9 s, 8.3 s, 8.7 s, 9.4 s and 9.8 s. Images are in pairs comparing the value at each time in the cycle between the initial duct and the duct with coarse interpolated inclined duct entry boundary condition.

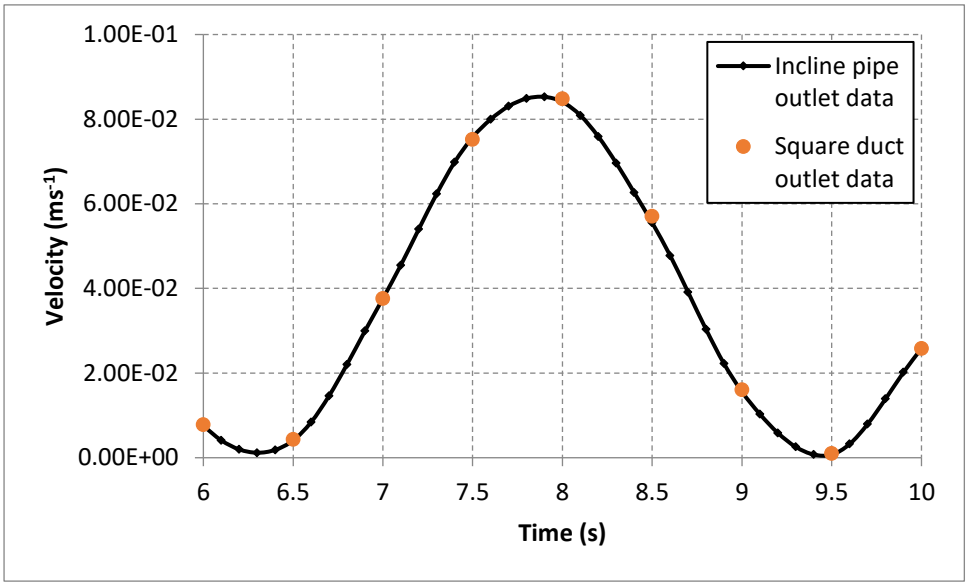

Figure 5 Variation of average velocity at outlet of original pipe and inclined pipe demonstrating that the boundary velocity interpolated from the initial model from sparse data is consistent with the solution original model driven by the source boundary condition function.

3 Application of 4D Local RBF Algorithm to Medical Imaging Data

Following validation on an analytical function, we now apply the 4D local RBF technique to uniformly spaced, 4-dimensional voxel-based MR measurements of cerebrospinal fluid (CSF) flow velocity in the cerebral lateral ventricles of the brain, acquired at consistent time intervals over the cardiac cycle.

Representative MRI data was acquired through the University of Nottingham Centre for Magnetic Resonance Imaging consisting of measurements of CSF flow velocity in all 3 component directions (u, v, w) at 62 horizontal slices through the brain of a healthy 25-year-old over a cardiac cycle. Image acquisition was configured to give the best available spatial and temporal resolution of the flow field, using a hybrid fast field echo sequence. Pulse oximetry gating was used to acquire 12 image sets over the cardiac cycle, (~1s) at 0.083s intervals. An in-plane voxel size of 1.79 by 1.79 mm with 2.4mm spacing between planes was used, with a field of view of 200mm x 200mm, giving a total dataset of 9,332,736 points. An initial acquisition with 50 mms^{-1} velocity encoding indicated peak lateral ventricular velocities of ~1-3 mms^{-1}. Therefore, to capture the flow field with adequate resolution and high signal to noise whilst avoiding aliasing, a velocity encoding of 5mms^{-1} was selected. Limitations of the technology mean that it is inevitable that some information lying between pixels is lost. Despite this, the speed of CSF flow (in the order of mm/s) relative to the pixel size means interpolation will give a reasonably accurate representation of the flow behaviour given a suitable number of input points. To avoid errors arising due to bulk movements of the human subject in the scanner over time, a linear least-square approximation of this rigid body motion was used. This enabled successful removal of erroneous velocities. Rigid body velocities were generally an order of magnitude less than that registered in the main body of fluid. Prior to rigid body motion removal, to investigate the sensitivity of the MRI velocity measurements to noise, several regions of expected zero velocity in the brain tissue where there is no flow other than diffusion (subject to rigid body motion) were captured in regions of approximately 10 by 10 voxels on a number of planes of interest. The standard deviation of the velocity data was 0.06 mm/s, 0.06 mm/s on the x- and y-directions on a sample of 2304 voxels. For the data reported in our results we estimate that the x-and y-velocities reported have an accuracy of $\pm$0.06 mm/s. We do not report the z-direction velocities here.

To demonstrate the interpolation, the number of output locations was increased to double the number of original datapoints, proportionally distributed in each direction (x,y,z,t). Figure 6 and Figure 7 show the application of the 4D RBF algorithm to the MRI dataset. In Figure 6, spatial interpolation is shown at a single point in the cardiac cycle. Two original planes are shown alongside a third intermediate location, which is not part of the original dataset. The number of pixel locations in the new, interpolated plane is increased fourfold. The complex variation of the flow field is reconstructed by the interpolation function and a clear smoothing between pixels is visible relative to the baseline images. The additional vectors and refined volume elements in Figure 6b) are consistent with the original images a) and c) producing a gradient of the velocity dependent on the RBF.

Application of the local 4-dimensional interpolation enables a prediction of the flow velocity magnitude and direction to be made at any location within the field over a cardiac cycle. Figure 7 demonstrates the effect of the interpolation in the temporal dimension. The original time steps of the MRI scan are reproduced on the left-hand column of images, but also including the spatial interpolation. The column of images on the right is not available in the original MRI data. The RBF interpolation produces intermediate time images which improve the visualisation of the temporal evolution of the flow field as it develops in the cardiac cycle. The improvement in the image rate from 12 per second to 24 per second provides a video rate observation of the cardiac cycle. The pattern of the velocity vectors is seen to vary in magnitude and direction during the cycle indicating pulsation of the flow. This refined dataset can improve understanding and visualisation of the physical interaction between the CSF and the cardiac rhythm.

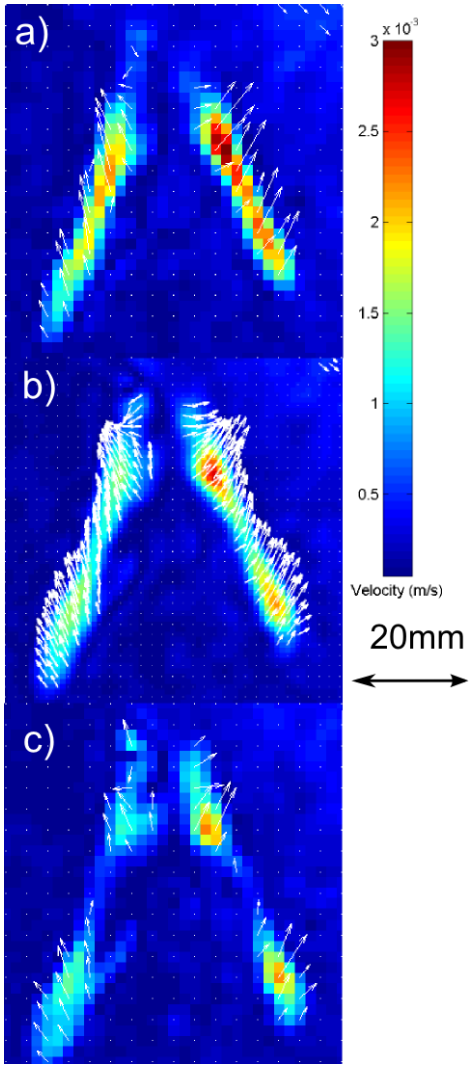

Figure 6 Interpolation of velocity magnitude (colour bar from 0 to 0.003 m/s) of cerebrospinal fluid in voxels from MRI scan with 3 Tesla machine, and 1.79mm voxels. The result of the interpolation is shown by comparing the original data with the interpolated image; a) original, at arbitrary height z which shows a section of the cerebral lateral ventricles, c) original data, at z – 1.79 mm and b) interpolated, at $z - \frac{1.79}{2}$ *mm. In this case the RBF interpolation has doubled the number of voxels in all 4 dimensions, i.e.* $2^4 = 16$ *times the number of voxels in the original (x, y, z, t) data set.*

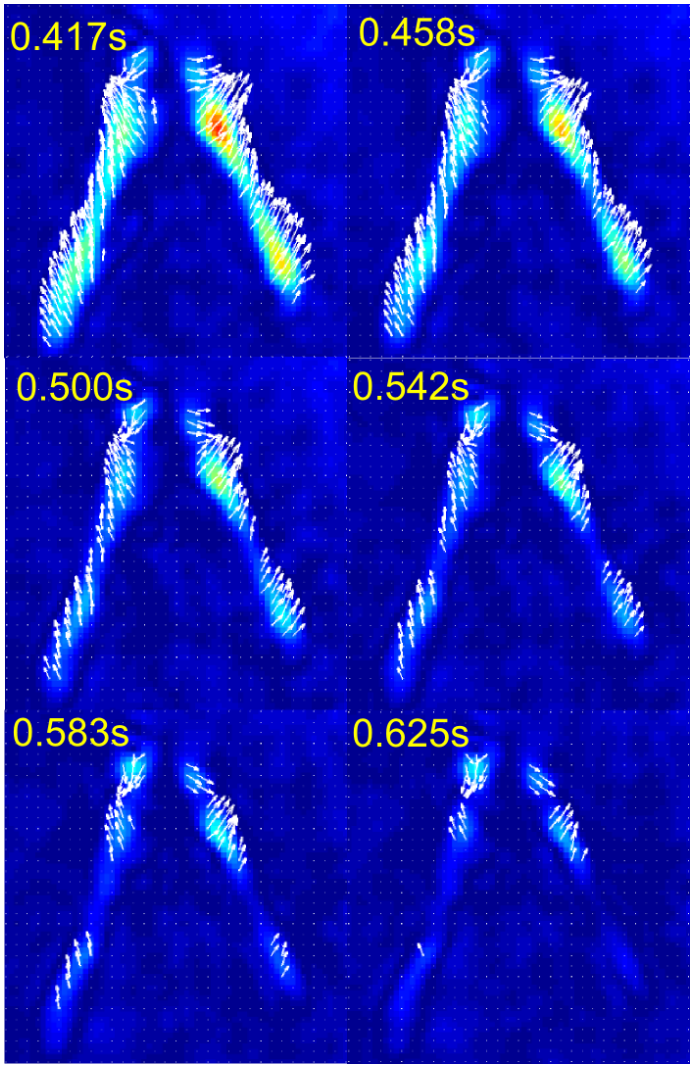

Figure 7 6 interpolated images from MRI scan with 3 Tesla machine, and Δt=0.083 s. Left hand images are at original time points and right-hand images are interpolated. The images are interpolated spatially and where there were only 12 time frames in the MRI, there are 24 time frames in the interpolated data, with Δt = 0.083/2 s. The colour bar from Figure 4 again applies to the velocity magnitude.

4 Discussion

The results of Section 2 demonstrate that the use of the 4D local multiquadric RBF formulation can provide a more computationally efficient, accurate and stable reconstruction of a known 4D function from a large dataset (of the order several hundred thousand points) when compared with a higher order polynomial based approach. This has not previously been achieved due to the tendency towards high computational cost and ill conditioning using global multiquadric RBF techniques. Restriction of the local stencil sizes in our method means that the number of data points never gets large enough for ill conditioning to become a problem. The partition of unity weighting applied to the local templates reduces the effect of heavily skewed outliers in the data. The algorithm ran on a 2 GHz dual core processor in the order of seconds, enabling rapid processing of results.

Having demonstrated the efficacy of the technique on a known function, we then showed that it could be used in real world applications for interpolation of complex, large scale (~several million points),

multidimensional physiological imaging datasets. The results in Section 3 show the 4D local RBF image interpolation offers a means of reconstructing velocities within a volume of CSF at data points intermediate to those available from the spatial resolution of the MRI scan and temporal resolution of cardiac gating, or which cannot be acquired without significantly increased scan times, causing stress on the subject and the MRI resource. It is also independent of the plane orientation of the image stack. Interpretation of anatomical definition of for example, tissue boundaries is a further possibility. 4D prediction of the entire velocity field could in future assist in determining medical diagnoses and optimal timing of drug delivery into the cerebrospinal fluid [1], [2], [3], [4], [5]. The efficient run times and lack of need for training on or knowledge of prior datasets may facilitate use of the algorithm in clinical settings, where rapid interpretation of results is important.

It would be of interest to further verify the robustness and applicability of the technique to a wider variety of MR Velocimetry data from both healthy and pathological cases and different locations within the CSF, such as the spinal cavity. Similarly, this work has not considered haemodynamic flows, which would typically require a divergence free condition to be applied, such as in [34]. It is not yet clear if the local RBF method described can predict haemodynamic flows without significant noise or be made compatible with the divergence free approach without loss of efficiency or stability. To facilitate this, future work will aim to expand the range of known analytical functions the technique is evaluated on to those representing transient turbulent flows, for example, the unsteady Hill's spherical vortex [Arzani]. The effect of varying the amount of random Gaussian noise on the raw dataset will also be investigated.

As for any interpolation, accuracy of the reconstruction produced is limited by the resolution of the original image data. Overly coarse MR velocimetry data can contain partial volume errors, whereby velocity recorded at a given spatial location contains signal from both stationary and moving tissues, for example, at fluid-tissue boundaries. In each application, care is needed to ensure an adequate balance between the increased data acquisition time required to achieve greater pixel resolution and accuracy of the interpolated 4D flow field. As a result, our method may not currently allow for accurate prediction from sparse or incomplete datasets such as maybe achieved using a machine learning approach. More work is required to determine the limitations of the technique in this respect, that is, at what sparsity of data does the level of accuracy of the interpolation appreciably deteriorate? An additional subject of future work may also be to harness the benefits of the multidimensional local RBF approach as part of, or in combination with a neural network algorithm to predict flow distribution of sparse datasets based on historical records and further reduce overall imaging time.

Comparison of the 4D RBF technique with results from a numerical model of the CSF flow region would provide further validation that it outperforms other potential multidimensional interpolation methods for this application. An alternative would be to create a synthetic 4D flow dataset from this CFD model to test the interpolation, similar to prior studies [38]. This would involve superimposing voxels from the MRI dataset onto the CFD mesh, then spatially averaging the data inside each voxel and adding Gaussian noise. However, the complexity of accurately modelling the influence of the pulsatile wall boundaries, due to the microscopic flow pulsations driving the flow, means a direct simulation of the CSF flow field has been discounted at this preliminary stage. Previous investigation of cerebrospinal fluid highlighted that flow passages in the cerebral ventricles are narrow (~1 cm) and the boundaries strongly influence flow behaviour. [5] suggested a method for estimating this pulsatile motion using spline interpolation of 2D MRI slices to predict volumetric change over the cardiac cycle. However, to accurately capture the magnitude of pulsation driving the flow at the flexible fluid-tissue ventricle wall boundary requires the application of a transiently and spatially varying velocity profile derived from the MR data. Therefore, an accurate derivation of boundary conditions in itself necessitates the use

of a 4D interpolation technique to map the wall boundary location and fluid and tissue motion at any point over the cardiac cycle. Figure 6 b) shows example locations on the boundary at close to zero flow velocity, indicating the most likely position of the ventricle wall at that cycle point can be predicted from the RBF interpolation. However, due to the small-scale movements involved, signal from these regions is particularly sensitive to partial volume effects and further work is needed to optimise the image acquisition procedure to achieve higher resolution at the wall boundaries.

Fluid mechanics can also be directly applied to analysis of an MR velocimetry dataset. In [48], the curl of a 4D MR velocity vector field is calculated, enabling the pressure field to be determined through the Navier-Stokes equations. However, the result of this manipulation is still a discrete rather than continuous dataset. [41] has significantly improved on this idea with a machine learning technique. Coupling our interpolation routine with this type of approach would be of significant interest as it would enable prediction of fluid pressure as well as velocity throughout the domain without the need for a numerical model, paving the way towards a complete, real-time prediction of pathological or healthy flow behaviour.

5 Conclusions

A preliminary evaluation of a 4-dimensional local radial basis function (RBF) algorithm for the interpolation of uniformly spaced, small-scale data, such as that derived from medical imaging has been presented. The validity of the subroutine has been demonstrated through interpolation of a known 4D function. The performance of the algorithm has been shown to be highly favourable in comparison with a quad-linear interpolation of the same dataset, demonstrating a significant improvement in accuracy and convergence rate.

The application of the interpolation tool has been demonstrated through reconstruction of a complex spatially and temporally varying 4-dimensional flow field derived from medical imaging data of cerebrospinal fluid flow in the brain. The results demonstrate that the technique offers an effective reconstruction of the flow field and could serve as a useful tool in the analysis of such datasets.

The 4-dimensional interpolation technique will be further validated through application to a greater range of analytical and medical imaging velocimetry problems such as turbulent haemodynamic flows. Use of the tool for the development of improved 4-dimensional boundary conditions for numerical models will be investigated. Coupling of the algorithm with a neural network-based approach will also be explored. This technique could then assist in the development of more physically realistic models of biological flow fields based on medical image data and hence improve understanding of the differences between healthy and pathological states.

Acknowledgements: The authors would like to thank the Engineering and Physical Sciences Research Council for funding the project (grant reference EP / P50354X/1) and supporting cross - disciplinary research. The continuing relationship with the Children's Brain Tumour Research Centre based at the Queen's Medical Centre provides the on-going incentive to drive this research effort. We dedicate this paper to the memory of our friend and colleague, Professor Henry Power, who inspired many PhD students.

6 Bibliography

[1] D. R. Enzmann and N. J. Pelc, “Brain motion: measurement with phase-contrast MR

imaging.," *Radiology*, vol. 185, no. 3, pp. 653–660, Dec. 1992, doi: 10.1148/radiology.185.3.1438741.

[2] U. Klose, C. Strik, C. Kiefer, and W. Grodd, "Detection of a relation between respiration and CSF pulsation with an echoplanar technique.," *J. Magn. Reson. Imaging*, vol. 11, no. 4, pp. 438–444, Apr. 2000, doi: 10.1002/(sici)1522-2586(200004)11:4<438::aid-jmri12>3.0.co;2-o.

[3] O. Balédent, M. C. Henry-Feugeas, and I. Idy-Peretti, "Cerebrospinal fluid dynamics and relation with blood flow: a magnetic resonance study with semiautomated cerebrospinal fluid segmentation.," *Invest. Radiol.*, vol. 36, no. 7, pp. 368–377, Jul. 2001, doi: 10.1097/00004424-200107000-00003.

[4] A. A. Linninger *et al.*, "Pulsatile cerebrospinal fluid dynamics in the human brain.," *IEEE Trans. Biomed. Eng.*, vol. 52, no. 4, pp. 557–565, Apr. 2005, doi: 10.1109/TBME.2005.844021.

[5] D. C. Zhu, M. Xenos, A. A. Linninger, and R. D. Penn, "Dynamics of lateral ventricle and cerebrospinal fluid in normal and hydrocephalic brains.," *J. Magn. Reson. Imaging*, vol. 24, no. 4, pp. 756–770, Oct. 2006, doi: 10.1002/jmri.20679.

[6] R. Franke, "Scattered Data Interpolation: Tests of Some Method," *Math. Comput.*, vol. 38, no. 157, pp. 181–200, Jun. 1982, doi: 10.2307/2007474.

[7] M. Bozzini, M. and Rossini, "Testing Methods for 3D Scattered Data Interpolation," *Monogr. la Acad. Ciencias Zaragoza*, vol. 20, pp. 111–13, 2002.

[8] R. L. Hardy, "Multiquadric equations of topography and other irregular surfaces," *J. Geophys. Res.*, vol. 76, no. 8, pp. 1905–1915, Mar. 1971, doi: 10.1029/JB076i008p01905.

[9] U. Ponzini, R., Biancolini, M.E., Rizzo, G., Morbiducci, "Computational Modelling of Objects Represented in Images," in *Computational Modelling of Objects Represented in Images*, DiGiamberardino et al., Ed. Taylor and Francis, 2012.

[10] J. Ringenberg, J. Deo, M. Devabhaktuni, V. Berenfeld, O. Snyder, B. Boyers, P. and Gold, "Accurate reconstruction of 3D cardiac geometry from coarsely-sliced MRI," *Comput. Methods Programs Biomed.*, vol. 113, pp. 483–493, 2014.

[11] A. Paiement, M. Mirmehdi, X. Xie, and M. C. K. Hamilton, "Integrated Segmentation and Interpolation of Sparse Data," *IEEE Trans. Image Process.*, vol. 23, no. 1, pp. 110–125, 2014, doi: 10.1109/TIP.2013.2286903.

[12] M. T. Rostami, M. Ezoji, R. Ghaderi, and J. Ghasemi, "Brain MRI segmentation using the mixture of FCM and RBF neural network," in *2013 8th Iranian Conference on Machine Vision and Image Processing (MVIP)*, 2013, pp. 425–429, doi: 10.1109/IranianMVIP.2013.6780023.

[13] Z. Chao and H.-J. Kim, "Slice interpolation of medical images using enhanced fuzzy radial basis function neural networks," *Comput. Biol. Med.*, vol. 110, pp. 66–78, 2019, doi: https://doi.org/10.1016/j.compbiomed.2019.05.013.

[14] W. R. Madych and S. A. Nelson, "Multivariate Interpolation and Conditionally Positive Definite Functions. II," *Math. Comput.*, vol. 54, no. 189, pp. 211–230, Jun. 1990, doi: 10.2307/2008691.

[15] R. Schaback, "Multivariate interpolation and approximation by translates of a basis function.," in *Approximation Theory VIII.*, L. Chui, C., Schumaker, Ed. London: World Scientific Publishing, 1995.

[16] Z. Wu, "Compactly supported positive definite radial functions," *Adv. Comput. Math.*, vol. 4,

no. 1, p. 283, 1995, doi: 10.1007/BF03177517.

[17] H. Wendland, “Error Estimates for Interpolation by Compactly Supported Radial Basis Functions of Minimal Degree,” *J. Approx. Theory*, vol. 93, no. 2, pp. 258–272, 1998, doi: https://doi.org/10.1006/jath.1997.3137.

[18] D. Brown, L. Ling, E. Kansa, and J. Levesley, “On approximate cardinal preconditioning methods for solving PDEs with radial basis functions,” *Eng. Anal. Bound. Elem.*, vol. 29, no. 4, pp. 343–353, 2005, doi: https://doi.org/10.1016/j.enganabound.2004.05.006.

[19] L. Ling and E. J. Kansa, “Preconditioning for radial basis functions with domain decomposition methods,” *Math. Comput. Model.*, vol. 40, no. 13, pp. 1413–1427, 2004, doi: https://doi.org/10.1016/j.mcm.2005.01.002.

[20] J. A. Muñoz-Gómez, P. González-Casanova, and G. Rodriguez-Gómez, “Domain Decomposition by Radial Basis Functions for Time Dependent Partial Differential Equations,” in *Proceedings of the 2nd IASTED International Conference on Advances in Computer Science and Technology*, 2006, pp. 105–109.

[21] A. H. Rosales and H. Power, “Non-Overlapping Domain Decomposition Algorithm for the Hermite Radial Basis Function Meshless Collocation Approach: Applications to Convection Diffusion Problems,” *J. Algorithm. Comput. Technol.*, vol. 1, no. 1, pp. 127–159, Jan. 2007, doi: 10.1260/174830107780122685.

[22] M. S. Ingber, C. S. Chen, and J. A. Tanski, “A mesh free approach using radial basis functions and parallel domain decomposition for solving three-dimensional diffusion equations,” *Int. J. Numer. Methods Eng.*, vol. 60, no. 13, pp. 2183–2201, Aug. 2004, doi: 10.1002/nme.1043.

[23] R. K. Beatson, W. A. Light, and S. Billings, “Fast Solution of the Radial Basis Function Interpolation Equations: Domain Decomposition Methods,” *SIAM J. Sci. Comput.*, vol. 22, no. 5, pp. 1717–1740, May 2000, doi: 10.1137/S1064827599361771.

[24] C. K. Lee, X. Liu, and S. C. Fan, “Local multiquadric approximation for solving boundary value problems,” *Comput. Mech.*, vol. 30, no. 5, pp. 396–409, 2003, doi: 10.1007/s00466-003-0416-5.

[25] A. I. Tolstykh and D. A. Shirobokov, “On using radial basis functions in a ‘finite difference mode’ with applications to elasticity problems,” *Comput. Mech.*, vol. 33, no. 1, pp. 68–79, 2003, doi: 10.1007/s00466-003-0501-9.

[26] E. Divo and A. J. Kassab, “An Efficient Localized Radial Basis Function Meshless Method for Fluid Flow and Conjugate Heat Transfer,” *J. Heat Transfer*, vol. 129, no. 2, pp. 124–136, 2006, doi: 10.1115/1.2402181.

[27] D. Stevens, H. Power, M. Lees, and H. Morvan, “A local hermitian RBF meshless numerical method for the solution of multi-zone problems,” *Numer. Methods Partial Differ. Equ.*, vol. 27, no. 5, pp. 1201–1230, Sep. 2011, doi: 10.1002/num.20577.

[28] D. Stevens, H. Power, M. Lees, and H. Morvan, “A Meshless Solution Technique for the Solution of 3D Unsaturated Zone Problems, Based on Local Hermitian Interpolation with Radial Basis Functions,” *Transp. Porous Media*, vol. 79, no. 2, pp. 149–169, 2009, doi: 10.1007/s11242-008-9303-z.

[29] C. A. Bustamante Chaverra, H. Power, W. F. Florez Escobar, and A. F. Hill Betancourt, “Two-

Dimensional Meshless Solution of the Non-Linear Convection-Diffusion-Reaction Equation by the Local Hermitian Interpolation Method ," *Ingeniería y Ciencia* , vol. 9. scieloco , pp. 21–51, 2013.

[30] Y. V. S. S. Monysekar, K. and Sanyasiraju, "An Upwind Scheme to Solve Unsteady Convection-Diffusion Equations Using Radial Basis Function Based Local Hermitian Interpolation Method with PDE Centres," *Procedia Eng.*, vol. 127, pp. 418–423, 2015.

[31] H.-F. Chan and C.-M. Fan, "The Local Radial Basis Function Collocation Method for Solving Two-Dimensional Inverse Cauchy Problems," *Numer. Heat Transf. Part B Fundam.*, vol. 63, no. 4, pp. 284–303, Apr. 2013, doi: 10.1080/10407790.2013.772004.

[32] Z. H. Wang, Z. Huang, W. Zhang, and G. Xi, "A Meshless Local Radial Basis Function Method for Two-Dimensional Incompressible Navier-Stokes Equations," *Numer. Heat Transf. Part B Fundam.*, vol. 67, no. 4, pp. 320–337, Apr. 2015, doi: 10.1080/10407790.2014.955779.

[33] R. Cavoretto, "A numerical algorithm for multidimensional modeling of scattered data points," *Comp. Appl. Math.*, vol. 34, pp. 65–80, 2015, doi: 10.1007/s40314-013-0104-9.

[34] P. Cavoretto, R. Schneider, T. and Zulian, "OPENCL Based Parallel Algorithm for RBF-PUM Interpolation," *J Sci Comput*, vol. 74, pp. 267–289, 2018, doi: https://doi.org/10.1007/s10915-017-0431-x.

[35] R. Cavoretto, "Adaptive Radial Basis Function Partition of Unity Interpolation: A Bivariate Algorithm for Unstructured Data," *J. Sci. Comput.*, vol. 87, p. 41, 2021, doi: https://doi.org/10.1007/s10915-021-01432-z.

[36] J. Thewlis, "Numerical Modelling of Cerebrospinal Fluid Flow in the Human Ventricular System based on 4-Dimensional Radial Basis Function Interpolation of MRI Data," University of Nottingham, 2013.

[37] P. Casa, L. and Krueger, "Radial basis function interpolation of unstructured, three-dimensional, volumetric particle tracking velocimetry data.," *Meas. Sci. Technol.*, vol. 24, no. 6, pp. 1–19, 2013.

[38] M. Zhou, X. Papadopoulou, V. Hau Leow, C. Vincent, P. and Tang, "3-d flow Reconstruction using divergence-free interpolation of multiple 2-d contrast-enhanced ultrasound particle imaging velocimetry measurements," *Ultrasound Med. Biol.*, vol. 45, no. 3, pp. 795–810, 2019.

[39] J. Busch, D. Giese, L. Wissmann, and S. Kozerke, "Reconstruction of divergence-free velocity fields from cine 3D phase-contrast flow measurements.," *Magn. Reson. Med.*, vol. 69, no. 1, pp. 200–210, Jan. 2013, doi: 10.1002/mrm.24221.

[40] W. Xiao, Z. Du, N. Liu, J. and Zhang, "SR-Net: A sequence offset fusion net and refine net for undersampled multislice MR image reconstruction," *Comput. Methods Programs Biomed.*, vol. 202, pp. 1–13, 2021.

[41] R. Fathi, M. Perez-Raya, I. Baghaie, A. Berg, P. Janiga, G. Arzani , A. and D'Souza, "Super-resolution and denoising of 4D-Flow MRI using physics-Informed deep neural nets.," *Comput. Methods Programs Biomed.*, vol. 197, pp. 1–16, 2020.

[42] E. J. Kansa, "A strictly conservative spatial approximation scheme for the governing engineering and physics equations over irregular regions and inhomogeneously scattered nodes," *Comput. Math. with Appl.*, vol. 24, no. 5–6, pp. 169–190, 1992, doi: https://doi.org/10.1016/0898-1221(92)90047-L.

[43] Y. C. Kansa, E J. and Hon, “Circumventing the ill-conditioning problem with multiquadric radial basis functions: Applications to elliptic partial differential equations,” *Comput. Math. with Appl.*, vol. 39, no. 7–8, pp. 123–137, 2000, doi: https://doi.org/10.1016/S0898-1221(00)00071-7.

[44] H. Golbabai, A. Mohebianfar, E. and Rabiei, “On the new variable shape parameter strategies for radial basis functions,” *Comp. Appl. Math.*, vol. 34, pp. 691–704, 2015, doi: 10.1007/s40314-014-0132-0.

[45] Y. D. Cavoretto, R. De Rossi, A. Mukhametzhanov, M.S. and Sergeyev, “On the search of the shape parameter in radial basis functions using univariate global optimization methods,” *J. Glob. Optim.*, vol. 79, pp. 305–327, 2021, doi: https://doi.org/10.1007/s10898-019-00853-3.

[46] A. H. Rosales, “Development of a numerical model describing the crystallisation process from an oversaturated solution of mineral gypsum in a porous media,” University of Nottingham, 2005.

[47] S. Arzani, A. and Dawson, “Data-driven cardiovascular flow modelling: examples and opportunities,” *J. R. Soc. Interface*, vol. 18, 2021, doi: 10.1098/rsif.2020.0802.

[48] S. Yatsushiro, A. Hirayama, M. Matsumae, and K. Kuroda, “Visualization of pulsatile CSF motion separated by membrane-like structure based on four-dimensional phase-contrast (4D-PC) velocity mapping.,” *Conf. Proc. ... Annu. Int. Conf. IEEE Eng. Med. Biol. Soc. IEEE Eng. Med. Biol. Soc. Annu. Conf.*, vol. 2013, pp. 6470–6473, 2013, doi: 10.1109/EMBC.2013.6611036.